1 Bacteriophage-embedded and coated alginate layers inhibit biofilm formation by

2 clinical strains of *Klebsiella pneumoniae*

3

4 Hala R. Ali [1,2], Carlos Valdivia [3], David Negus [1*]

5

6 [1] Department of Biosciences, Nottingham Trent University, United Kingdom

7 [2] Animal Health Research Institute, Agriculture Research Centre, Egypt

8 [3] Institute for Integrative Systems Biology, University of Valencia-CSIC, Paterna,

9 Spain

10

11 [*] **Corresponding author**: Department of Biosciences, Nottingham Trent University,

12 Clifton Campus, Clifton Lane, Nottingham NG11 8NS, UK. E-mail

13 david.negus@ntu.ac.uk;

14

15 **Abbreviations**: AMR, antimicrobial resistance; EPS, extracellular polysaccharide;

16 KL, capsule locus; PBS, phosphate buffered saline; ST, sequence type; TSA,

17 tryptone soy agar; TSB, tryptone soy broth.

18

19 **Keywords**: multidrug-resistant, AMR, biofouling

20

21 **Running title**: Bacteriophage alginate layers

22   **ABSTRACT**

23   AIMS

24   This study aimed to determine the antibiofilm properties of *Klebsiella pneumoniae*

25   phages previously isolated from Thai hospital sewage water. Furthermore, we aimed

26   to develop a phage-embedded and coated alginate hydrogel, suitable as a wound

27   dressing or surface coating to prevent *K. pneumoniae* proliferation and biofilm

28   formation.

29   METHODS AND RESULTS

30   The biofilm forming capacity of six clinical *K. pneumoniae* isolates was determined

31   by means of the crystal violet assay and four strains which exhibited strong

32   adherence were selected for further characterisation. Two phages

33   (vB_KpnA_GBH014 and vB_KpnM_GBH019) were found to both significantly

34   prevent (P = <0.0005) and disrupt (P = <0.05) biofilms produced by their *K.*

35   *pneumoniae* hosts as determined by optical density readings using the crystal violet

36   assay. Furthermore, alginate layers embedded and coated with phages

37   vB_KpnA_GBH014 and vB_KpnM_GBH019 produced antibiofilm surfaces. Viable

38   counts of recovered biofilms showed that alginate hydrogels containing phage

39   vB_KpnA_GBH014 or vB_KpnM_GBH019 were associated with significantly fewer

40   *K. pneumoniae* versus no-phage controls (1.61×10^8 cfu ml^{-1} vs 1.67×10^4 cfu ml^{-1},

41   P = <0.005 and 1.78×10^8 cfu ml^{-1} vs 6.11×10^2 cfu ml^{-1}, P = <0.00005,

42   respectively). Confocal microscopy further revealed a significant reduction in the

43   biovolume of biofilms formed on phage embedded and coated alginate hydrogels

44   compared to no-phage controls.

45

46

47 <u>CONCLUSIONS</u>

48 Phages vB_KpnA_GBH014 and vB_KpnM_GBH019 can both prevent and disrupt

49 biofilms produced by clinical isolates of *K. pneumoniae*. Embedding and coating

50 these phages into alginate produces an antibiofilm matrix which may have promise

51 for coating medical devices or as a wound dressing.

52 <u>IMPACT STATEMENT</u>

53 *K. pneumoniae* is an important drug-resistant pathogen and a major cause of

54 hospital acquired infections. Biofilm formation is considered a major virulence factor,

55 allowing *K. pneumoniae* to adhere to abiotic surfaces. Here we demonstrate that lytic

56 phages of *K. pneumoniae* are effective antibiofilm agents and can be formulated into

57 alginate hydrogels as potential wound dressings or surface coatings.

58

59

INTRODUCTION

Klebsiella pneumoniae is an escalating global health threat attributed to 10% of

nosocomial infections (Tesfa et al. 2022). Transmission in a healthcare setting can

occur via contaminated respirators, catheters, and invasive surgeries in acute care

facilities (Chang et al. 2021). Of particular concern are extended-spectrum β-

lactamase-producing strains of *K. pneumoniae*, such as those expressing the KPC

β-lactamase which hydrolyses a range of frontline antibiotics including carbapenems

(Arnold et al. 2011). The situation is further exacerbated by the emergence of

hypervirulent *K. pneumoniae* strains which can cause conditions including

meningitis, pyogenic liver abscesses and pneumonia in otherwise healthy individuals

outside of a healthcare setting (Russo et al. 2024).

Biofilm formation by *K. pneumoniae* is recognised as an important virulence factor

(Guerra et al. 2022). Existence of cells in a biofilm has shown to correlate with

decreased susceptibility to a range of antibiotics (Anderl et al. 2000, Singla et al.

2013, Tang et al. 2020, Karimi et al. 2021). This effect has been partly attributed to

the biofilm providing a physical barrier which reduces the penetration of some

antibiotics and thus prevents the drug from reaching its intended target [6-9].

Moreover, biofilm production facilitates attachment and persistence on abiotic

surfaces, such as indwelling medical devices (Di Martino et al. 2003, Schroll et al.

2010, Stahlhut et al. 2012). The polysaccharide capsule of *K. pneumoniae* forms an

important component of the biofilm and more than 130 different capsule types have

been identified by genetic analysis (Follador et al. 2016). Capsule production has

been implicated in protection from complement mediated lysis (Dolores Álvarez et al.

2000, Jensen et al. 2020) although its precise role remains unclear (Loraine et al.

2018). Capsular and extracellular polysaccharides contribute to the architecture of

85   the *K. pneumoniae* biofilm (Dzul et al. 2011) and are thought to play an important

86   role in initial adhesion to surfaces and maturation of the biofilm (Balestrino et al.

87   2008).

88   Owing to the recalcitrant nature of *K. pneumoniae* and its biofilms to traditional

89   antibiotic chemotherapy, new modalities for preventing or perturbing biofilms caused

90   by this opportunistic pathogen should be explored. Bacteriophages, hereafter

91   referred to as phages, are viruses that infect and kill bacteria. They are highly

92   selective agents, typically acting on individual strains or closely related species of

93   bacteria. In addition, phages encode a range of gene products, such as

94   depolymerase enzymes, which selectively hydrolyse polysaccharides found in

95   bacterial capsules and biofilms (Hughes et al. 1998, Harper et al. 2014, Pires et al.

96   2016). As such, phages show promise for the prevention and eradication of biofilms,

97   such as those which occur on indwelling medical devices. Previous studies have

98   investigated the potential of incorporating phages of *Salmonella* and *Escherichia coli*

99   in an alginate matrix for therapeutic purposes (Moghtader et al. 2017, Colom et al.

100   2017, Zhou et al. 2022, Shiue et al. 2022). These studies have primarily focused on

101   encapsulating phage in alginate for improved stability during transit of the

102   gastrointestinal tract following oral delivery. As biofilm formation is a key virulence

103   factor of *K. pneumoniae*, we wished to develop an alginate / phage formulation that

104   would act as an antibiofilm coating for medical devices or could potentially be utilised

105   as a wound dressing. Here, we test the antibiofilm properties of a selection of

106   phages previously isolated from Thai hospital sewage water (Blundell-Hunter et al.

107   2021) against a collection of *K. pneumoniae* strains cultured from hospital patients,

108   including multi-drug-resistant isolates (Loraine et al. 2018). Our results are therefore

109   highly translatable and have direct clinical relevance.

110

MATERIALS AND METHODS

Strain and cultivation information

113   *K. pneumoniae* isolates used in this study were originally isolated and characterised

114   by Lorraine *et al*., [16] and were a kind gift from Professor Peter Taylor, University

115   College London, UK. Briefly, *K. pneumoniae* isolates were cultured from blood, urine,

116   pus, sputum, and ascitic fluid samples at the clinical microbiology laboratories of

117   three tertiary care hospitals in Thailand. Strains with prefix TU were isolated from

118   Thammasat University Hospital, strains with prefix SR were isolated from Siriraj

119   Hospital and strains with prefix SG were isolated from Songklanagarind Hospital.

120   Bacteria were identified by routine biochemical tests for identification of Gram-

121   negative bacteria. Details of all bacterial strains used in this study can be found in

122   **Table 1.** Antibiotic susceptibility testing was performed using the VITEK 2 system

123   (BioMerieux) and the results can be found in **Table 2**. Phages vB_KpnA_GBH014

124   (GBH014) and vB_KpnM_GBH019 (GBH019) were originally isolated by Blundell-

125   Hunter *et al*., (Blundell-Hunter et al. 2021). Genome sequence data for GBH014 and

126   GBH019 is available at NCBI under accessions OU342754 and OU509535

127   respectively. GBH014 was propagated on *K. pneumoniae* SR10 whereas GBH019

128   was propagated on strain SG41. All bacterial strains were grown on tryptone soy

129   agar (TSA, Fisher Scientific) unless stated otherwise. Tryptone soy broth (TSB,

130   Fisher Scientific) was used for overnight cultures which were incubated aerobically at

131   37 °C with shaking (160 rpm). All media used for phage assays were supplemented

132   with $CaCl_2$ and $MgCl_2$ (both at final concentration of 0.5 mol^{-3}).

133

134 **Bioinformatic analyses of *K. pneumoniae* strains**

135 Genome assemblies for *K. pneumoniae* strains were downloaded as FASTA files

136 from NCBI and uploaded to the Pathogenwatch website, available at

137 https://pathogen.watch/ (Argimón et al. 2021). The integrated Kleborate tool v2.2.0

138 (Lam et al. 2021) was used for prediction of capsule locus (KL), sequence type (ST),

139 antimicrobial resistance (AMR) genes and the presence of genes associated with the

140 hypermucoviscous phenotype.

141

142 **Bioinformatic analyses of phages**

143 Phages GBH014 and GBH019 were analysed for their therapeutic suitability using

144 the online PhageLeads tool (Yukgehnaish et al. 2022) which detects genes involved

145 in lysogeny and the presence of antimicrobial resistance or virulence genes.

146 Genome sequences in FASTA format were uploaded to the web tool located at

147 https://phageleads.dk/

148

149 **Biofilm assays and their interpretation**

150 Biofilm assays were performed as described previously (Stepanovic et al. 2000,

151 Merritt et al. 2011, Eladawy et al. 2021). In brief, a single colony of each strain was

152 used to inoculate 5 ml of TSB. Cultures were incubated aerobically for 24 h at 37 °C

153 with shaking (160 rpm). The overnight cultures were adjusted to an optical density of

154 0.2 at a wavelength of 600 nm (OD_{600}) in TSB. Aliquots (100 µl) of the diluted

155 cultures were introduced into wells of a 96-well plate. The plates were incubated

156 aerobically for 24 h at 37 °C without shaking. Following incubation, spent medium
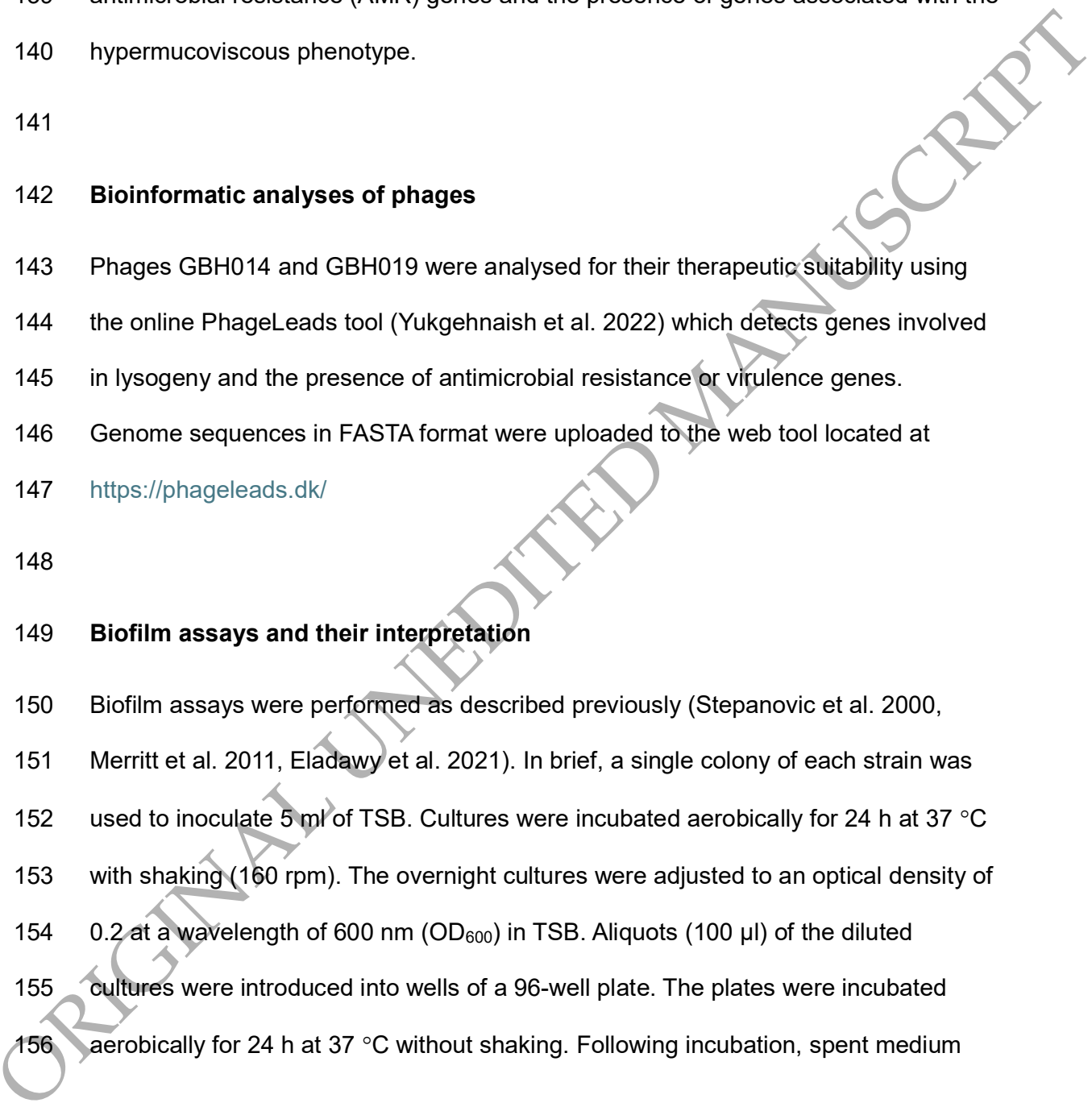
157   was carefully removed from each well and the wells were washed three times with

158   200 µl sterile phosphate-buffered saline (pH 7.4; Oxoid) to remove any non-adherent

159   planktonic cells. The adherent cells were fixed by heat treatment at 60 °C for 60 min

160   to prevent widespread detachment of biofilms prior to dye staining. The adhered

161   biofilms were then stained by addition of 1% crystal violet (Sigma-Aldrich, 150 µl per

162   well) and the 96-well plate was left to incubate for 20 min. Excess stain was carefully

163   removed from the wells and discarded. The 96-well plate was then carefully rinsed

164   with distilled water three times, and the plate inverted and left at room temperature

165   until the wells were dry. Stained biofilms were solubilised by adding 33 % (v/v) glacial

166   acetic acid (Sigma-Aldrich) to each well (150 µl per well). After solubilisation of the

167   stained biofilms, the OD_{540} was measured and recorded for all samples using a

168   BioTek Cytation $|^3$ imaging reader spectrophotometer. Uninoculated medium was

169   used as a negative control in biofilm assays. Biological (n=3) and technical (n=4)

170   replicates were performed for all strains. The mean of each isolate's OD

171   quadruplicate readings (OD_i) was calculated and compared with the control cut-off

172   OD (OD_C), which was defined as three standard deviations (SD) above the mean of

173   the negative control (3SD + mean). The amount of biofilm formed was scored as

174   non-adherent ($OD_i \leq OD_C$), weakly adherent ($OD_C < OD_i \leq 2\,OD_C$), moderately

175   adherent ($2\,OD_C < OD_i \leq 4\,OD_C$) or strongly adherent ($4\,OD_C < OD_i$). Statistical

176   significance of the differences in biofilm formation was assessed using unpaired t

177   test.

178

180 **Phage–biofilm assays**

181 The titre of each phage stock was determined by plaque assay using the double-

182 layer agar technique. Briefly, each phage was serially diluted in phosphate-buffered

183 saline (pH 7.4; Oxoid) and 100 µl phage dilution (10^{-1} to 10^{-9}) was combined with

184 100 µl of an overnight culture of the corresponding *K. pneumoniae* host used for

185 routine phage propagation and 5 ml of 0.6 % TSA supplemented with $CaCl_2$ and

186 $MgCl_2$ both at a final concentration of 0.5 mol^{-3}. The mixture was gently swirled and

187 poured onto solid TSA plates. Plates were incubated overnight at 37 °C and plaque

188 forming units per ml (pfu ml^{-1}) determined by enumeration of visible plaques.

189 The ability of each phage to prevent and disrupt biofilms was examined using a

190 modification of a previously described protocol (Taha et al. 2018). We define

191 prevention as the ability of phage to prevent the formation of a new biofilm and

192 disruption as the capacity of phage to reduce the biomass of an already established

193 biofilm. For prevention of biofilms, host cultures were incubated aerobically for 24 h

194 at 37 °C with shaking (160 rpm) in TSB. Overnight cultures were diluted to an OD_{600}

195 of 0.2 and aliquots (100 µl) of diluted culture were introduced into wells of a 96-well

196 plate. Phages (100 µl) were added to treated wells at a final concentration of 7 x 10^9

197 pfu ml^{-1}. Untreated control wells had 100 µl of TSB added. Plates were incubated

198 without shaking for 24 h at 37 °C. Then, the supernatants were discarded, the biofilm

199 of each well was washed to remove planktonic cells and biofilms stained as

200 described above.

201 To investigate the disruption of established biofilms, host cultures were grown and

202 prepared as described above prior to inoculating a 96-well plate. Plates were

179

203 incubated without shaking for 24 h at 37 °C to allow biofilms to form. Unattached

204 planktonic cells were carefully aspirated without disrupting the biomass. Phages

205 were added to test wells at a final concentration of 7×10^9 pfu ml^{-1}, whereas control

206 wells received only TSB (100 µl) without phage. Plates were incubated for a further

207 24 h at 37 °C without shaking. Supernatants were carefully discarded; the biofilm of

208 each well was washed to remove planktonic cells and biofilms stained as described

209 above. Biological (*n*=3) and technical (*n*=4) replicates were completed for all strains.

210 Statistical significance of the differences in the amount of biofilm between conditions

211 was assessed using unpaired *t* test.

212

213 **Phage-coated and embedded alginate hydrogels**

214 Phage-coated and embedded alginate layers were created based on the method

215 described by Shiue *et al*., (Shiue et al. 2022) by conjugating phage to the bottom and

216 top of an alginate hydrogel containing embedded phage. Briefly, 100 µl of phage

217 stock (GBH014 at 1×10^{13} pfu ml^{-1}, or GBH019 at 2.22×10^{13} pfu ml^{-1}) was added to

218 the bottom of a 96-well plate. Phage-embedded alginate mixture was prepared by

219 combining 200 µl of phage (at aforementioned concentrations) with 800 µl of 4%

220 (w/v) alginate solution and the mixture (100 µl per well) was carefully distributed to

221 wells of the 96-well plate containing phage. The top surface of the alginate was

222 conjugated by carefully adding 100 µl of phage stock onto the alginate layer and the

223 gel was crosslinked by the addition of calcium chloride/HEPES buffer (pH 7.5) to a

224 final concentration of 1.5% / 1.3 mol^{-4} respectively. After 10 minutes, the alginate gel

225 was rinsed twice with 200 µl 1.3 mol^{-4} HEPES buffer (pH 7.5) to remove any phage

226 not conjugated to the bottom or top of the crosslinked alginate.

Antibiofilm assays

Phage-coated and embedded alginate hydrogels were inoculated with 200 µl of *K. pneumoniae* overnight culture adjusted to an OD_{600} 0.2. Alginate hydrogels without phage were used as a non-treatment control. The 96-well plate was placed in a static incubator at 37°C for 24 h and the bacterial inoculum carefully removed. The alginate gel was carefully rinsed twice (100 µl per well, per wash) with phosphate buffered saline (PBS) to remove any planktonic cells. The number of viable cells in the biofilm was enumerated by disrupting the alginate gel in the well via the addition of 200 µl 0.5 mol^{-1} sodium citrate dihydrate (pH 6) and the mixture transferred to 800 µl of µl 0.5 mol^{-1} sodium citrate dihydrate (pH 6) followed by vigorous vortexing. The disrupted gel was serially diluted in PBS and cfu ml^{-1} counts performed by the method of Miles and Misra (Miles et al. 1938). Biological (*n*=4) and technical (*n*=3) replicates were completed for all strains. Statistical significance of the differences in bacterial counts between conditions was assessed using unpaired *t* test.

Effect of alginate on phage infectivity

To determine if embedding phage GBH014 or GBH019 in alginate affected the viability of the phage, we calculated the lytic titre of each phage before and after alginate treatment. Phage GBH014 and GBH019 (both at 1×10^9 pfu ml^{-1}) were embedded in alginate by combining 100 µl of phage stock with 400 µl of 4% (w/v) alginate solution. The mixture (100 µl per well) was carefully distributed to wells of a 96-well plate in triplicate and the gel was crosslinked by the addition of calcium chloride/HEPES buffer (pH 7.5) to a final concentration of 1.5%/ 1.3 mol^{-4} respectively. Alginate gels were disrupted in the well via the addition of 100 µl 0.5

251   mol^{-1} sodium citrate dihydrate (pH 6) and the mixture was serially diluted in TSB to

252   determine the pfu ml^{-1} using the double agar plaque assay. To ensure the process of

253   disrupting the gel with sodium citrate dihydrate had no effect on phage viability, we

254   included a control of phage treated with only the crosslinking agent of calcium

255   chloride/1.3 mol^{-4} HEPES buffer and 0.5 mol^{-1} sodium citrate dihydrate used to

256   disrupt the gel. Biological (n=3) and technical (n=3) replicates were completed for

257   each condition. Statistical significance of the difference in pfu ml^{-1} between the three

258   conditions was determined by a one-way ANOVA (Kruskal-Wallis).

259

260   **Phage release from alginate**

261   Phage embedded and conjugated alginate gels were created by adding 400 µl of

262   phage GBH014 or GBH019 (both at $1x10^9$ pfu ml^{-1}) to the bottom of a 24-well plate.

263   Phage-embedded alginate mixture was prepared by combining 260 µl of phage (at

264   aforementioned concentrations) with 1040 µl of 4% (w/v) alginate solution and the

265   mixture (400 µl per well) was carefully distributed to wells of the 24-well plate

266   containing phage. The top surface of the alginate was conjugated by carefully adding

267   400 µl of phage stock onto the alginate layer and the gel was crosslinked by the

268   addition of calcium chloride/HEPES buffer (pH 7.5) to a final concentration of

269   1.5%/1.3 mol^{-4} respectively. After 10 minutes, alginate gels were rinsed twice with

270   750 µl 1.3 mol^{-4} HEPES buffer (pH 7.5) to remove any non-conjugated phage. The

271   number of phage particles released from the gel was measured by adding PBS (1

272   ml) to each well. After 0, 2, 6 and 24 h the 1 ml PBS was collected and replaced with

273   the same amount of fresh PBS. Wells containing alginate at 0 h were dissolved by

274   the addition of sodium citrate to determine the initial total titre (N_0) of phage. The

275 number of phage particles in the collected PBS or dissolved alginate was determined

276 by serial dilution and double agar plaque assay. The percentage of lytic phage

277 released over time was calculated as (cumulative total of released phage particles /

278 N_0) X 100%. Biological (*n*=3) and technical (*n*=3) replicates were completed for each

279 phage).

280

281 **Confocal laser scanning microscopy and image analysis**

282 For the visualisation of biofilms, phage-coated and embedded alginate hydrogels

283 and no-phage controls were prepared in 96-well plates as described above. Briefly,

284 80 µl of phage stock ($1x10^9$ pfu ml^{-1}, both GBH014 and GBH019) was added to the

285 bottom of a 96-well plate. Phage-embedded alginate mixture was prepared by

286 combining 200 µl of phage (at aforementioned concentration) with 800 µl of 4% (w/v)

287 alginate solution and the mixture (140 µl per well) was carefully distributed to wells of

288 the 96-well plate containing phage. The top surface of the alginate was conjugated

289 by carefully adding 80 µl of phage stock onto the alginate layer and crosslinking and

290 washing was performed as described above. Phage-coated and embedded alginate

291 hydrogels were inoculated with 100 µl of *K. pneumoniae* overnight culture adjusted

292 to an OD_{600} 0.2. Alginate hydrogels without phage were used as a non-treatment

293 control. The 96-well plate was placed in a static incubator at 37°C for 24 h and the

294 bacterial inoculum carefully removed. The alginate gel was carefully rinsed twice

295 (100 µl per well, per wash) with PBS to remove any planktonic cells. Biofilms were

296 stained by the addition of 200 µl LIVE/DEAD™ *Bac*Light™ stain (Fisher Scientific)

297 prepared according to manufacturer's instructions. Stained biofilms were incubated

298 in the dark at room temperature for 10 min and the stain carefully aspirated. Alginate

299 layers were then carefully inverted and transferred to the wells of a CELLview cell

300 culture slide (Greiner). Microscopy was performed using a Leica TCS SP5 confocal

301 microscope with a 40x water objective (444 nm excitation, green emission and 555

302 nm excitation, red emission). All images were deconvolved with Huygens Essential

303 version 22.10 (Scientific Volume Imaging, The Netherlands, http://svi.nl), using the

304 CMLE algorithm for a numerical aperture of 1.4 and water as embedding media.

305 Maximum intensity projections were produced using LASX 3.10.0 software (Leica).

306 The best images were selected to illustrate this work and are representative of the

307 entire observed sample. Biovolume of the biofilm was calculated using Imaris

308 v10.2.0 (Oxford Instruments), where the biovolume was calculated as the sum of

309 volumes of each individual cell in the Z-stack. Biovolumes represent the mean of

310 acquisitions from three independent images for each sample.

311

312 **RESULTS**

313 This study aimed to develop an alginate hydrogel containing phages against *K.*

314 *pneumoniae* which would provide an antibiofilm matrix with applications in coating

315 medical devices or as a potential wound dressing. To achieve this aim, we first

316 identified *K. pneumoniae* isolates capable of forming strong (4 OD_C < OD_i) biofilms

317 by testing a panel of clinical strains containing multi-drug-resistant isolates (**Table 1**

318 **and Table 2**).

319

320 **Biofilm-forming ability of strains used in this study**

321 The *K. pneumoniae* clinical strains used in this study were isolated from hospitals in

322 Thailand and described previously Loraine *et al*., (Loraine et al. 2018) and are

323   described in further detail in **Table 1** and **Table 2**. We determined the biofilm-forming

324   ability of these [33]and found that all the isolates could form either moderate (2 OD_C

325   < OD_i ≤ 4 OD_C) or strong (4 OD_C < OD_i) biofilms (**Figure 1; Supplementary Table**

326   **1**). All strains which produced strong biofilms (SR10, SR3, SG41 and TU1) were

327   taken forward for further analysis whereas the two isolates which formed moderate

328   biofilms (SR4 and TU16) were excluded from further study.

329

330   **Capacity of phages to prevent and disrupt *K. pneumoniae* biofilms**

331   Phages GBH014 and GBH019 were selected for characterisation as they had

332   previously been shown to lyse all four *K. pneumoniae* isolates identified as strong

333   biofilm formers in the current study (SR10 / SR3 lysed by GBH014; and SG41 / TU1

334   lysed by GBH019) (Blundell-Hunter et al. 2021). However, their antibiofilm properties

335   have not previously been determined. We therefore examined their capacity to

336   prevent (**Figure 2, Supplementary table 2**) and disrupt (**Figure 3, Supplementary**

337   **table 3**) biofilms produced by the four "strong" biofilm producers.

338   Phage GBH014 was found to be highly effective at preventing biofilms formed by *K.*

339   *pneumoniae* SR10. There was a highly significant ($P < 0.005$) difference in biofilm

340   formation between phage-treated and non-treated controls. GBH014 was less

341   effective at preventing biofilms formed by *K. pneumoniae* SR3, although there was

342   still a significant ($P < 0.05$) reduction in the amount of biofilm formed by this isolate in

343   the presence of GBH014. Presence of phage GBH019 significantly ($P < 0.0005$)

344   reduced the amount of biofilm formed by *K. pneumoniae* SG41. However, GBH014

345   was unable to significantly reduce biofilm formation by *K. pneumoniae* TU1

346   compared to no-phage controls.

347   The ability of the phages to disrupt pre-established biofilms was investigated using

348   strain SR10 for phage GBH014 and SG41 for phage GBH019. These strains were

349   selected as they were the most sensitive to biofilm prevention by their respective

350   phages. Addition of either GBH014 to *K. pneumoniae* to SR10 or GBH019 to *K.*

351   *pneumoniae* SG41 significantly ($P < 0.05$) disrupted biofilms formed by these clinical

352   isolates.

353

354   **Antibiofilm properties of phage-embedded and coated alginate hydrogels**

355   We prepared alginate hydrogels embedded and coated with phages according to the

356   method described by Shiue *et al.,* (Shiue et al. 2022) and investigated their

357   antibiofilm properties compared to alginate hydrogels containing no phage (**Figure 4,**

358   **supplementary table 4**). Alginate hydrogels containing either phage GBH014 or

359   GBH019 were found to significantly ($P < 0.05$) prevent biofilm formation by their

360   respective *K. pneumoniae* host strains SR10 and SG41 compared to alginate layers

361   which did not contain phage. Alginate hydrogels containing either phage were able to

362   reduce the bioburden of *K. pneumoniae* biofilms by several orders of magnitude.

363   Specifically, viable counts of recovered biofilms showed that alginate hydrogels

364   containing phage GBH014 or GBH019 were associated with significantly fewer *K.*

365   *pneumoniae* versus no-phage controls (1.61×10^8 cfu ml^{-1} vs 1.67×10^4 cfu ml^{-1}, $P =$

366   <0.005 and 1.78×10^8 cfu ml^{-1} vs 6.11×10^2 cfu ml^{-1}, $P = <0.00005$, respectively). In

367   the case of hydrogels containing phage GBH019 and inoculated with *K. pneumoniae*

368   SG41, two biological repeats resulted in enumerations below our limit of detection of

369   100 cfu ml^{-1}.

370 To visualise the antibiofilm properties of the phage-embedded and coated alginate

371 layers, we used confocal laser scanning microscopy in combination with live/dead

372 staining (**Figure 5**). Prior to microscopy, biofilms were treated with *Bac*Light™

373 (Fisher Scientific) which stains viable cells green and dead cells red. Visual

374 inspection of representative areas of stained biofilms revealed that in accordance

375 with cfu ml^{-1} counts, there was a visibly large reduction in the number of viable cells

376 present in biofilms formed on alginate hydrogels containing either phage GBH014 or

377 GBH019 (Figure 5A and 5C). In comparison, alginate layers which did not contain

378 phage were found to be coated with dense biofilms of almost confluent *K.*

379 *pneumoniae* cells (Figure 5B and 5D). Biofilms formed on alginate in the absence of

380 phage were found to extend throughout the entire 15 µm of the Z-stack (the

381 maximum measurable distance), whereas we were unable to visualise the presence

382 of biofilm in many areas of samples coated and embedded with phage. To help

383 quantify the amount of representative biofilm present, we calculated the total

384 biovolume of each biofilm via image analysis **(Supplementary table 5)**. The mean

385 biovolume of the biofilm formed b*y K. pneumoniae* SR10 in the absence of phage

386 was 712232 µ^3 compared to a biovolume of 30029 µ^3 on alginate containing phage

387 SR10 (approximately 24-fold reduction). Similarly, *K. pneumoniae* SG41 formed a

388 biofilm with a mean biovolume of 554060 µ^3 in the absence of phage compared to a

389 mean biovolume of 31730 µ^3 on alginate coated and embedded with phage GBH019

390 (approximately 17-fold reduction).

391

392

Effect of alginate on phage infectivity and release of phage from alginate

hydrogels

To determine if treatment with alginate negatively affected the lytic capacity of the

phages used in this study, we calculated the lytic titre of each phage before and after

incorporation into an alginate hydrogel. We found there was a less than one-log

reduction in pfu ml^{-1} for either phage following alginate treatment compared to non-

treated controls (**Figure 6a, supplementary table 6**). This relatively small reduction

in viability was found not to be statistically significant ($P > 0.05$; one-way ANOVA,

Kruskal-Wallis). We also saw that treatment with either calcium chloride or sodium

citrate dihydrate (the reagents used to crosslink and disrupt the alginate gels,

respectively) had minimal effect on phage viability.

We found that the release of the two phages from alginate hydrogels differed

significantly **(Figure 6b, Supplementary table 7)**. Phage GBH014 appeared to be

more readily released from the gel, with approximately 6% of the total phage

incorporated released almost immediately. This release continued steadily with

approximately 40% of the total phage released by 24 h. Contrarily, the release of

GBH019 was slower and more limited. A minimal percentage of phage were initially

released (0.6% at 0 h) with approximately 15% of the total phage incorporated being

released by 24 h.

412

DISCUSSION

Increasing rates of drug-resistance identified in *K. pneumoniae* has necessitated the

investigation of alternative treatment strategies for this important pathogen. Reports

416 of extensively drug resistant (Huang et al. 2018, Li, L. et al. 2019) and pan-drug

417 resistant strains of *K. pneumoniae* (Kaur, J. N. et al. 2024), means that in some

418 cases only a small number of treatment options remain available when relying on

419 traditional antibiotic chemotherapy. Investigations into alternative treatment options

420 for *K. pneumoniae* have included antimicrobial peptides (de Souza et al. 2022) efflux

421 pump inhibitors (Vieira Da Cruz et al. 2024) and depolymerase enzymes (Cai et al.

422 2023). Lytic phages have received significant research interest as an alternative

423 treatment for their potential to kill important antibiotic resistant strains of *K.*

424 *pneumoniae* (Herridge et al. 2020). Infections caused by this opportunistic pathogen

425 are often associated with indwelling medical devices, including urinary catheters

426 (Stahlhut et al. 2012, Liu et al. 2020), central venous catheters (Patil et al. 2011) and

427 ventilators (Yan et al. 2016, Guo, S. et al. 2016). Colonisation of abiotic surfaces,

428 such as catheters, by *K. pneumoniae* is facilitated by biofilm formation (Di Martino et

429 al. 2003) and as such, biofilm formation is often seen as the primary step of infection.

430 In addition to its role in attachment and persistence on abiotic surfaces, biofilm

431 production is also recognised to reduce susceptibility to important antibiotics (Anderl

432 et al. 2000, Singla et al. 2013, Tang et al. 2020, Karimi et al. 2021). As biofilm

433 formation is intimately linked to infection and drug-resistance, therapeutic

434 approaches which prevent colonisation should be considered a priority. We

435 investigated the potential of two phages (GBH014 and GBH019), previously isolated

436 from Thai sewage (Blundell-Hunter et al. 2021) to prevent and disrupt biofilms

437 formed by clinical isolates of *K. pneumoniae* and further characterised the antibiofilm

438 properties of an alginate hydrogel containing these phages.

439 The *K. pneumoniae* hosts used in this study had previously been isolated from

440 patients at tertiary hospitals in Thailand as part of a study investigating the

441 relationship between susceptibility to human complement and strain genome

442 sequence (Loraine et al. 2018). We initially determined the biofilm-forming ability of

443 these strains using a 96-well crystal violet assay and found that all isolates produced

444 moderate to strong biofilms, with strain SR10 producing the greatest amount of

445 biofilm. Further bioinformatic analyses of the isolates identified that SR10 harbours

446 the *rmpA* and *rmpD* genes (**Supplementary table 8**) associated with the

447 hypermucoviscous phenotype of hypervirulent strains (Nassif et al. 1989, Walker et

448 al. 2020). The clinical importance of the hypermucoviscous phenotype is debated, a

449 recent meta-analysis found no correlation between hypermucoviscous strains and

450 increased mortality in patients suffering from bacteraemia but did identify that

451 hypermucoviscousity was associated with an increased incidence of multiorgan

452 abscess formation (Namikawa et al. 2023). Similarly, others have found that

453 hypermucoviscousity is associated with increased cases of *K. pneumoniae* invasive

454 syndrome which encompasses liver abscess, meningitis, pleural empyaema,

455 endovascular lesions (e.g. mycotic aneurysm), or endophthalmitis (Lee et al. 2006).

456 Genes associated with the hypermucoviscous phenotype were absent from all other

457 strains included in our study. Furthermore, strain SR10 encodes the *rmpC* gene

458 which has been identified as an important regulator of capsule expression (Walker et

459 al. 2019). It has been reported previously that hypermucoviscous strains produce

460 more biofilm compared to classical *K. pneumoniae* strains (Kong et al. 2012) and our

461 finding, that SR10 produces the most biofilm compared to other strains included in

462 the study (**Figure 1**), supports the correlation between hypermucoviscousity and

463 biofilm formation.

464 To characterise the antibiofilm properties of our phages, we utilised the four *K.*

465 *pneumoniae* strains identified as strong biofilm formers (SR10, SR3, SG41 and

466 TU1). Phage GBH014 has previously been identified as lytic on hosts SR10 and SR3

467 (both capsule locus KL2) whereas phage GBH019 is known to infect SG41 and TU1

468 (both capsule locus KL102) (Blundell-Hunter et al. 2021). The infective range of

469 these phages is likely determined by the capsule type elaborated by the host, with

470 each phage infecting a limited number of K-types encoded by specific KL loci. This

471 specificity is often driven by the presence or absence of phage associated K-type

472 specific hydrolytic enzymes, often referred to as capsule depolymerases, which

473 selectively degrade this polysaccharide layer (Beamud et al. 2023). We confirmed

474 that each phage could lyse its reported host by means of a simple plaque assay

475 which results in zone of clearing on a bacterial lawn if a particular host is sensitive to

476 lysis (**Supplementary figure 1**). However, we observed that plaques produced by

477 GBH014 on SR3 where not as transparent as those produced by the same phage on

478 SR10 and that plaques produced by GBH019 on TU1 were not as clear as those

479 observed on host SG41. This correlates with the observations of Blundell-Hunter *et*

480 *al*., (Blundell-Hunter et al. 2021) who also reported partial lysis of strain TU1 by

481 phage GBH019. Turbid or translucent plaques can be indicative of lysogeny.

482 However, as our bioinformatic analysis was unable to identify any classical genes

483 associated with a temperate lifestyle for either phage, we do not believe this to be

484 the case. The observed difference in plaque morphologies may therefore be due to

485 inefficient lysis of the test strain compared to the routine propagation host. Moreover,

486 we found that phage GBH014 significantly reduced the amount of biofilm produced

487 by strain SR10 but was less effective against SR3. As these hosts share an identical

488 capsule locus (KL2) these differences are highly unlikely to be due to differing

489 capsule structures altering phage binding. Similarly, phage GBH019 varied in its

490 effectiveness to reduce biofilm formation by strains TU1 and SG41, two hosts which

491 also possess an identical capsule locus (KL102). To help account for the observed

492 differences in plaque morphologies and biofilm prevention, we determined the

493 relative efficiency of plating (EOP) for each phage by dividing the number of plaques

494 (titre) formed on its routine propagation host relative to the titre observed on a test

495 strain (**Supplementary table 9**). We found the relative EOP of phage GBH014 on

496 strain SR3 relative to its propagation host (SR10) to be significantly less (relative

497 EOP 0.00000095). Similarly, the relative EOP of GBH019 on strain TU1 was

498 considerably lower compared to its routine propagation host (relative EOP 0.0082).

499 The reduced plating efficiencies observed for each phage on strains other than their

500 propagation host likely explains why they were relatively infective at preventing

501 biofilm formation by these strains.

502 Prevention of biofilm formation in these experiments is highly likely to result from

503 direct lysis of hosts. Disruption of established biofilms is more challenging. Mature

504 biofilms have complex architecture, often containing protein, nucleic acids and

505 extracellular polysaccharides (Rather et al. 2021). We found that phages GBH014

506 and GBH019 could significantly reduce the biomass of established biofilms produced

507 by *K. pneumoniae* strains SR10 and SG41 respectively. The capacity of phages to

508 disrupt established biofilms, which are primarily composed of extracellular

509 polysaccharides (EPS), has been attributed to the action of phage-associated

510 depolymerase enzymes which hydrolyse the polymer leading to subsequent infection

511 and lysis of host cells (Hughes et al. 1998, Gutiérrez et al. 2015, Guo, Z. et al. 2017,

512 Mi et al. 2019). Previous bioinformatic analysis of the genomes of GBH014 and

513 GBH019 identified the presence of several potential depolymerase enzymes

514 (Blundell-Hunter et al. 2021). Depolymerases were identified on the basis amino acid

515 similarity by comparing the translated genomes of GBH014 and GBH019 against a

516   curated a database of 25 published phage-encoded *K. pneumoniae* capsule

517   depolymerases. The authors identified two potential depolymerases encoded within

518   the genome of GBH014 and eight within the genome of the jumbo-phage GBH019. It

519   is possible that these depolymerases play a role in the observed disruption of

520   established biofilms. Others have also reported that biofilms produced by *Klebsiella*

521   spp. can be disrupted by either the action of phages which encode potential

522   depolymerase enzymes (Ku et al. 2021, Zurabov et al. 2023) or using purified

523   depolymerase in the absence of phage particles (Wu et al. 2019, Latka and Drulis-

524   Kawa 2020, Li, M. et al. 2021, Sun et al. 2023).

525   To help determine the therapeutic suitability of phages GBH014 and GBH019, their

526   genomes were analysed using the online tool PhageLeads. PhageLeads detects

527   genes involved in lysogeny, and the presence of antimicrobial resistance or virulence

528   genes. Phages which have the potential to undergo lysogeny (incorporation of their

529   genome into the host chromosome) are undesirable for therapeutic use due to the

530   potential for the movement of host related genes as part of the lysogenic lifestyle.

531   Neither phage were found to possess genes related to lysogeny, AMR or virulence

532   factors and therefore represent suitable therapeutic candidates.

533   As established biofilms are typically difficult to remove and recalcitrant to

534   chemotherapy, the formulation of phage into a coating to create a biofouling-resistant

535   surface could be highly beneficial in preventing biofilm formation in important settings

536   such as indwelling medical devices. We investigated the potential of using the

537   biopolymer, alginate, to create a phage-embedded and coated surface which such

538   properties. Alginate is a polysaccharide composed of D-mannuronic acid and L-

539   guluronic acid. When exposed to divalent cations (such as Ca^{+2} in the present study)

540   alginate forms a cross-linked matrix with the capacity to trap phages within the three-

541 dimensional network. The polymer can be either directly incorporated into a medical

542 device such a catheter through 3D printing (Archana et al. 2023) or used to coat

543 surfaces via a range of methods including dip (Xiao et al. 2009) coating or spin

544 coating (Vakili and Asefnejad 2020). Phages embedded in alginate have been shown

545 to possess enhanced stability (Colom et al. 2017, Moghtader et al. 2017, Silva

546 Batalha et al. 2021) and can aid in controlled release of virus particles (Colom et al.

547 2017, Silva Batalha et al. 2021). Alginate has already been extensively investigated

548 as a potential wound dressing due to its biocompatibility and lack of toxicity (Paul

549 and Sharma 2004, Zhang and Zhao 2020). Additionally, there are examples in the

550 literature of the potential to incorporate or coat medical devices or implants with

551 alginate in combination with antimicrobials to prevent biofilm formation (Lv et al.

552 2014, Archana et al. 2023, Yang et al. 2024).

553 In the present study, alginate layers embedded and coated with either phage

554 GBH014 or GBH019 were found to significantly inhibit biofilm formation by *K.*

555 *pneumoniae* compared to alginate layers which did not contain phage. The potential

556 to incorporate phage into alginate preparations, either as a drug delivery system or

557 an antibacterial coating, has been investigated for phages against a range of

558 pathogens including, *Staphylococcus aureus* (Ma et al. 2012)*, Escherichia coli* (Silva

559 Batalha et al. 2021, Shiue et al. 2022)*, Salmonella* Typhimurium (Colom et al. 2017)

560 and *Pseudomonas aeruginosa* (Chen et al. 2023). Kaur *et al.,* incorporated a *K.*

561 *pneumoniae* phage into a polyvinyl alcohol-Sodium alginate hydrogel as part of a

562 multi-phage preparation which also included phages against *S. aureus* and *P.*

563 *aeruginosa.* (Kaur, P. et al. 2019). Alternative methods for encapsulating phage for

564 enhanced delivery or immobilisation have been investigated. These approaches

565 include use of alternative polymers such as chitosan and polyvinyl alcohol

566   (Choińska-Pulit et al. 2015). Additionally, liposomes (spherical vesicles composed of

567   one or more phopsolipid bilayers) have been used to encapsulate phage.

568   Encapsulation of *Klebsiella* phages in liposomes has been shown to improve

569   retention of virus particles at the infection site and improve efficacy in a murine burn

570   model (Chadha et al. 2017). Phages can also be immobilised with fibres to create

571   "bioactive surfaces". Such fibres are often produced by electrospinning and phages

572   can be embedded into the fibres during the process. This technique has the

573   advantage of producing a material which is soft, flexible and porous and therefore

574   represents an attractive option for producing wound dressings (Loh et al. 2021). All

575   the aforementioned strategies possess their own unique advantages and

576   disadvantageous and a number of reviews are available on this topic (Choińska-Pulit

577   et al. 2015, Loh et al. 2021, Pardo-Freire and Domingo-Calap 2023). We believe that

578   alginate hydrogels represent one of the most attractive options primarily due to the

579   ease with which they can be created. The process requires little to no specialist

580   equipment and therefore phage embedded hydrogels can be produced in settings

581   with limited resources. We also found that incorporating either phage into alginate

582   had minimal effect on phage viability. This finding further supports the use of alginate

583   as a substrate for phage immobilisation and release.

584   Interestingly, we observed that the release kinetics for the of the two phages was

585   markedly different. Phage GBH014 was quickly released from the alginate gel with

586   an initial burst of phage release (Approximately 20% by 4 h) followed by a more

587   steady release whereas phage GBH019 was released much more slowly from the

588   gel. The difference in the speed of release may be attributable to the different sizes

589   and morphologies of the two phages. Phage GBH019 is a "jumbo phage" with a

590   myovirus morphology, it has a capsid diameter of 133 nm and a tail length of 163

591 nm. Phage GBH014 has a podovirus morphology and is much smaller (capsid

592 diameter of 64 nm and a tail too short to measure accurately) (Blundell-Hunter et al.

593 2021). The larger size of both the capsid and tail of GBH019 may result in this phage

594 being released more slowly from the alginate matrix. It has been noted previously

595 that jumbo phages diffuse poorly in semi-solid media (Serwer et al. 2007). Others

596 have reported that the antibacterial effect of immobilised phages is primarily due to

597 the action of phages which are released from the matrix (Leppänen et al. 2019,

598 Shiue et al. 2022). We observed that both phages used in the current study were

599 highly effective at preventing biofilm formation when incorporated into alginate.

600 Although their release kinetics differed, it was observable that both phages were

601 continuing to be released from the matrix up to 24 h. This continuous release of

602 phage may contribute to the highly effective antibiofilm properties we observe in the

603 present study.

604 In summary, phages GBH014 and GBH019 show promise as antibiofilm agents

605 effective against clinically relevant strains of *K. pneumoniae*. Our results show that

606 these phages can both prevent and disrupt established biofilms and that their

607 incorporation into alginate hydrogels produces an antibiofilm substrate which shows

608 promise as a potential wound dressing or as an antimicrobial coating to prevent

609 biofouling of abiotic surfaces, such as those of indwelling medical devices. Future

610 studies should focus on the translation of these *in vitro* findings towards clinical use.

611 Properly controlled clinical trials should be conducted to validate the potential use of

612 phage-based treatments or preparations in medical settings.

613 **Acknowledgements**

619

620 **Conflicts of interest**

621 None declared.

622

623 **Data availability**

624 Genome sequences of the bacteriophages used in this study are available at NCBI

625 and their accession numbers can be found in in the methods section. Genome

626 sequences of the *K. pneumoniae* isolates are available at NCBI and their accession

627 numbers can be found in Table 1. Supporting data relating to all experiments are

628 available in the online supplementary material.

References

Anderl JN, Franklin MJ, Stewart PS. Role of Antibiotic Penetration Limitation in *Klebsiella pneumoniae* Biofilm Resistance to Ampicillin and Ciprofloxacin. *Antimicrob Agents Chemother* 2000; **44**, 1818–1824. https://doi.org/10.1128/AAC.44.7.1818-1824.2000.

Archana M, Rubini D, Dharshini KP, et al. Development of an anti-infective urinary catheter composed of polyvinyl alcohol/sodium alginate/methylcellulose/polyethylene glycol by using a pressure-assisted 3D-printing technique. *Int J Biol Macromol* 2023; **249**, 126029. https://doi.org/10.1016/j.ijbiomac.2023.126029.

Argimón S, David S, Underwood A, et al. Rapid Genomic Characterization and Global Surveillance of *Klebsiella* Using Pathogenwatch. *Clin Infect Dis* 2021; **73**, S325–S335. https://doi.org/10.1093/cid/ciab784.

Arnold RS, Thom KA, Sharma S, et al. Emergence of *Klebsiella pneumoniae* Carbapenemase-Producing Bacteria. *South Med J* 2011; **104**, 40–45. https://doi.org/10.1097/SMJ.0b013e3181fd7d5a.

Balestrino D, Ghigo J, Charbonnel N, et al. Characterization of functions involved in the establishment and maturation of *Klebsiella pneumoniae* in vitro biofilm reveals dual roles for surface exopolysaccharides. *Environ Microbiol* 2008; **10**, 685–701. https://doi.org/10.1111/j.1462-2920.2007.01491.x.

Beamud B, García-González N, Gómez-Ortega M, et al. Genetic determinants of host tropism in *Klebsiella* phages. *Cell Rep* 2023; **42**, 112048. https://doi.org/10.1016/j.celrep.2023.112048.

Blundell-Hunter G, Enright MC, Negus D, et al. Characterisation of Bacteriophage-Encoded Depolymerases Selective for Key *Klebsiella pneumoniae* Capsular Exopolysaccharides. *Front Cell Infect Microbiol* 2021; **11**, 686090. https://doi.org/10.3389/fcimb.2021.686090.

Cai R, Ren Z, Zhao R, et al. Structural biology and functional features of phage-derived depolymerase Depo32 on *Klebsiella pneumoniae* with K2 serotype capsular polysaccharides. *Microbiol Spectr* 2023; **11**, e0530422. https://doi.org/10.1128/spectrum.05304-22.

Chadha P, Katare OP, Chhibber S. Liposome loaded phage cocktail: Enhanced therapeutic potential in resolving *Klebsiella pneumoniae* mediated burn wound infections. *Burns* 2017; **43**, 1532–1543. https://doi.org/10.1016/j.burns.2017.03.029.

Chang D, Sharma L, Dela Cruz CS, et al. Clinical Epidemiology, Risk Factors, and Control Strategies of *Klebsiella pneumoniae* Infection. *Front Microbiol* 2021; **12**, 750662. https://doi.org/10.3389/fmicb.2021.750662.

667   Chen B, Benavente LP, Chittò M, et al. Alginate microbeads and hydrogels
668   delivering meropenem and bacteriophages to treat *Pseudomonas aeruginosa*
669   fracture-related infections. *J Control Release* 2023; **364**, 159–173.
670   https://doi.org/10.1016/j.jconrel.2023.10.029.

671   Choińska-Pulit A, Mituła P, Śliwka P, et al. Bacteriophage encapsulation: Trends
672   and potential applications. *Trends Food Sci Technol* 2015; **45**, 212–221.
673   https://doi.org/10.1016/j.tifs.2015.07.001.

674   Colom J, Cano-Sarabia M, Otero J, et al. Microencapsulation with
675   alginate/CaCO3: A strategy for improved phage therapy. *Sci Rep* 2017; **7**, 41441.
676   https://doi.org/10.1038/srep41441.

677   de Souza CM, da Silva ÁP, Júnior NGO, et al. Peptides as a therapeutic strategy
678   against *Klebsiella pneumoniae*. *Trends Pharmacol Sci* 2022; **43**, 335–348.
679   https://doi.org/10.1016/j.tips.2021.12.006.

680   Di Martino P, Cafferini N, Joly B, et al. *Klebsiella pneumoniae* type 3 pili facilitate
681   adherence and biofilm formation on abiotic surfaces. *Res Microbiol* 2003; **154**, 9–
682   16. https://doi.org/10.1016/S0923-2508(02)00004-9.

683   Dolores Álvarez, Susana Merino, Juan M. Tomás, et al. Capsular Polysaccharide
684   Is a Major Complement Resistance Factor in Lipopolysaccharide O Side Chain-
685   Deficient *Klebsiella pneumoniae* Clinical Isolates. *Infect Immun* 2000; **68**, 953.
686   https://doi.org/10.1128/IAI.68.2.953-955.2000.

687   Dzul SP, Thornton MM, Hohne DN, et al. Contribution of the *Klebsiella*
688   *pneumoniae* Capsule to Bacterial Aggregate and Biofilm Microstructures. *Appl*
689   *Environ Microbiol* 2011; **77**, 1777–1782. https://doi.org/10.1128/AEM.01752-10.

690   Eladawy M, El-Mowafy M, El-Sokkary MMA, et al. Antimicrobial resistance and
691   virulence characteristics in ERIC-PCR typed biofilm forming isolates of *P.*
692   *aeruginosa*. *Microb Pathog* 2021; **158**, 105042.
693   https://doi.org/10.1016/j.micpath.2021.105042.

694   Follador R, Heinz E, Wyres KL, et al. The diversity of *Klebsiella pneumoniae*
695   surface polysaccharides. *Microb Genom* 2016; **2**, e000073.
696   https://doi.org/10.1099/mgen.0.000073.

697   Guerra MES, Destro G, Vieira B, et al. *Klebsiella pneumoniae* Biofilms and Their
698   Role in Disease Pathogenesis. *Front Cell Infect Microbiol* 2022; **12**, 877995.
699   https://doi.org/10.3389/fcimb.2022.877995.

700   Guo S, Xu J, Wei Y, et al. Clinical and molecular characteristics of *Klebsiella*
701   *pneumoniae* ventilator-associated pneumonia in mainland China. *BMC Infect Dis*
702   2016; **16**, 1–7.

703

704

705   Guo Z, Huang J, Yan G, et al. Identification and Characterization of Dpo42, a
706   Novel Depolymerase Derived from the *Escherichia coli* Phage
707   vB_EcoM_ECOO78. *Front Microbiol* 2017; **8**, 1460.
708   https://doi.org/10.3389/fmicb.2017.01460.

709   Gutiérrez D, Briers Y, Rodríguez-Rubio L, et al. Role of the Pre-neck Appendage
710   Protein (Dpo7) from Phage vB_SepiS-phiIPLA7 as an Anti-biofilm Agent in
711   *Staphylococcal* Species. *Front Microbiol* 2015; **6**, 1315.
712   https://doi.org/10.3389/fmicb.2015.01315.

713   Harper D, Parracho H, Walker J, et al. Bacteriophages and Biofilms. *Antibiotics*
714   *(Basel)* 2014; **3**, 270–284. https://doi.org/10.3390/antibiotics3030270.

715   Herridge WP, Shibu P, O'Shea J, et al. Bacteriophages of *Klebsiella* spp., their
716   diversity and potential therapeutic uses. *J Med Microbiol* 2020; **69**, 176–194.
717   https://doi.org/10.1099/jmm.0.001141.

718   Huang Y, Chou S, Liang S, et al. Emergence of an XDR and carbapenemase-
719   producing hypervirulent *Klebsiella pneumoniae* strain in Taiwan. *J Antimicrob*
720   *Chemother* 2018; **73**, 2039–2046. https://doi.org/10.1093/jac/dky164.

721   Hughes KA, Sutherland IW, Jones MV. Biofilm susceptibility to bacteriophage
722   attack: the role of phage-borne polysaccharide depolymerase. *Microbiology* (Soc
723   Gen Microbiol) 1998; **144**, 3039–3047. https://doi.org/10.1099/00221287-144-11-
724   3039.

725   Jensen TS, Opstrup KV, Christiansen G, et al. Complement mediated *Klebsiella*
726   *pneumoniae* capsule changes. *Microbes Infect* 2020; **22**, 19–30.
727   https://doi.org/10.1016/j.micinf.2019.08.003.

728   Karimi K, Zarei O, Sedighi P, et al. Investigation of Antibiotic Resistance and
729   Biofilm Formation in Clinical Isolates of *Klebsiella pneumoniae*. *Int J Microbiol*
730   2021; 2021, 5573388–6. https://doi.org/10.1155/2021/5573388.

731   Kaur JN, Singh N, Smith NM, et al. Next generation antibiotic combinations to
732   combat pan-drug resistant *Klebsiella pneumoniae*. *Sci Rep* 2024; **14**, 3148.
733   https://doi.org/10.1038/s41598-024-53130-z.

734   Kaur P, Gondil VS, Chhibber S. A novel wound dressing consisting of PVA-SA
735   hybrid hydrogel membrane for topical delivery of bacteriophages and antibiotics.
736   *Int J Pharm* 2019; **572**, 118779. https://doi.org/10.1016/j.ijpharm.2019.118779.

737   Kong Q, Beanan JM, Olson R, et al. Biofilm formed by a hypervirulent
738   (hypermucoviscous) variant of *Klebsiella pneumoniae* does not enhance serum
739   resistance or survival in an in vivo abscess model. *Virulence* 2012; **3**, 309–318.
740   https://doi.org/10.4161/viru.20383.

741 Ku H, Kabwe M, Chan HT, et al. Novel Drexlerviridae bacteriophage KMI8 with
742 specific lytic activity against *Klebsiella michiganensis* and its biofilms. *PLoS One*
743 2021; **16**, e0257102. https://doi.org/10.1371/journal.pone.0257102.

744 Lam MMC, Wick RR, Watts SC, et al. A genomic surveillance framework and
745 genotyping tool for *Klebsiella pneumoniae* and its related species complex. *Nat*
746 *Commun* 2021; **12**, 4188–4188. https://doi.org/10.1038/s41467-021-24448-3.

747 Latka A, Drulis-Kawa Z. Advantages and limitations of microtiter biofilm assays in
748 the model of antibiofilm activity of *Klebsiella* phage KP34 and its depolymerase.
749 *Sci Rep* 2020; **10**, 20338–12. https://doi.org/10.1038/s41598-020-77198-5.

750 Lee H, Chuang Y, Yu W, et al. Clinical implications of hypermucoviscosity
751 phenotype in *Klebsiella pneumoniae* isolates: association with invasive syndrome
752 in patients with community-acquired bacteraemia. *J Intern Med* 2006; **259**, 606–
753 614. https://doi.org/10.1111/j.1365-2796.2006.01641.x.

754 Leppänen M, Maasilta IJ, Sundberg L. Antibacterial Efficiency of Surface-
755 Immobilized *Flavobacterium*-Infecting Bacteriophage. *ACS Appl Bio Mater* 2019;
756 **2**, 4720–4727. https://doi.org/10.1021/acsabm.9b00242.

757 Li L, Yu T, Ma Y, et al. The Genetic Structures of an Extensively Drug Resistant
758 (XDR) *Klebsiella pneumoniae* and Its Plasmids. *Front Cell Infect Microbiol* 2019;
759 **8**, 446. https://doi.org/10.3389/fcimb.2018.00446.

760 Li M, Li P, Chen L, et al. Identification of a phage-derived depolymerase specific
761 for KL64 capsule of *Klebsiella pneumoniae* and its anti-biofilm effect. *Virus Genes*
762 2021; **57**, 434–442. https://doi.org/10.1007/s11262-021-01847-8.

763 Liu X, Sai F, Li L, et al. Clinical characteristics and risk factors of catheter-
764 associated urinary tract infections caused by *Klebsiella pneumoniae*. *Ann Palliat*
765 *Med* 2020; **9**, 2668–2677. https://doi.org/10.21037/apm-20-1052.

766 Loh B, Gondil VS, Manohar P, et al. Encapsulation and Delivery of Therapeutic
767 Phages. *Appl Environ Microbiol* 2021; **87** https://doi.org/10.1128/AEM.01979-20.

768 Loraine J, Heinz E, De Sousa Almeida J, et al. Complement susceptibility in
769 relation to genome sequence of recent *Klebsiella pneumoniae* isolates from Thai
770 hospitals. *mSphere* 2018; **3** https://doi.org/10.1128/mSphere.00537-18.

771 Lv H, Chen Z, Yang X, et al. Layer-by-layer self-assembly of minocycline-loaded
772 chitosan/alginate multilayer on titanium substrates to inhibit biofilm formation. *J*
773 *Dent* 2014; **42**, 1464–1472. https://doi.org/10.1016/j.jdent.2014.06.003.

774 Ma Y, Pacan JC, Wang Q, et al. Enhanced alginate microspheres as means of
775 oral delivery of bacteriophage for reducing *Staphylococcus aureus* intestinal
776 carriage. *Food Hydrocoll* 2012; **26**, 434–440.
777 https://doi.org/10.1016/j.foodhyd.2010.11.017.

778 Merritt JH, Kadouri DE, O'Toole GA. Growing and Analyzing Static Biofilms. *Curr*
779 *Protoc Microbiol* (Online) 2011; **22**, 1B.1.1–1B.1.18.
780 https://doi.org/10.1002/9780471729259.mc01b01s22.

781 Mi L, Liu Y, Wang C, et al. Identification of a lytic *Pseudomonas aeruginosa*
782 phage depolymerase and its anti-biofilm effect and bactericidal contribution to
783 serum. *Virus Genes* 2019; **55**, 394–405. https://doi.org/10.1007/s11262-019-
784 01660-4.

785 Miles AA, Misra SS, Irwin JO. The estimation of the bactericidal power of the
786 blood. *Epidemiol Infect* 1938; **38**, 732–749.

787 Moghtader F, Eğri S, Piskin E. Phages in modified alginate beads. *Artif Cells*
788 *Nanomed Biotechnol* 2017; **45**, 357–363.
789 https://doi.org/10.3109/21691401.2016.1153485.

790 Namikawa H, Oinuma K, Yamada K, et al. Differences in severity of bacteraemia
791 caused by hypermucoviscous and non-hypermucoviscous *Klebsiella*
792 *pneumoniae*. *Int J Antimicrob Agents* 2023; **61**, 106767.
793 https://doi.org/10.1016/j.ijantimicag.2023.106767.

794 Nassif X, Fournier J, Arondel J, et al. Mucoid phenotype of *Klebsiella*
795 *pneumoniae* is a plasmid-encoded virulence factor. *Infect Immun* 1989; **57**, 546–
796 552. https://doi.org/10.1128/iai.57.2.546-552.1989.

797 Pardo-Freire M, Domingo-Calap P. Phages and Nanotechnology: New Insights
798 against Multidrug-Resistant Bacteria. *Biodes Res* 2023; **5**, 0004.
799 https://doi.org/10.34133/bdr.0004.

800 Patil HV, Patil VC, Ramteerthkar MN, et al. Central venous catheter-related
801 bloodstream infections in the intensive care unit. *Indian J Crit Care Med* 2011; **15**,
802 213–223. https://doi.org/10.4103/0972-5229.92074.

803 Paul W, Sharma CP. Chitosan and alginate wound dressings: a short review.
804 *Trends Biomater Artif Organs* 2004; **18**, 18–23.

805 Pires DP, Oliveira H, Melo LDR, et al. Bacteriophage-encoded depolymerases:
806 their diversity and biotechnological applications. *Appl Microbiol Biotechnol* 2016;
807 **100**, 2141–2151. https://doi.org/10.1007/s00253-015-7247-0.

808 Rather MA, Gupta K, Mandal M. Microbial biofilm: formation, architecture,
809 antibiotic resistance, and control strategies. *Braz J Microbiol* 2021; **52**, 1701–
810 1718. https://doi.org/10.1007/s42770-021-00624-x.

811 Russo TA, Alvarado CL, Davies CJ, et al. Differentiation of hypervirulent and
812 classical *Klebsiella pneumoniae* with acquired drug resistance. *mBio* 2024; **15**,
813 e0286723. https://doi.org/10.1128/mbio.02867-23.

814 Schroll C, Barken KB, Krogfelt KA, et al. Role of type 1 and type 3 fimbriae in
815 *Klebsiella pneumoniae* biofilm formation. *BMC Microbiol* 2010; **10**, 179–179.
816 https://doi.org/10.1186/1471-2180-10-179.

817 Serwer P, Hayes SJ, Thomas JA, et al. Propagating the missing bacteriophages:
818 a large bacteriophage in a new class. *Virol J* 2007; **4**, 21–21.
819 https://doi.org/10.1186/1743-422x-4-21.

820 Shiue S, Syu F, Lin H. Two types of bacteriophage-modified alginate hydrogels as
821 antibacterial coatings for implants. *J Taiwan Inst Chem Eng* 2022; **134**, 104353.
822 https://doi.org/10.1016/j.jtice.2022.104353.

823 Silva Batalha L, Pardini Gontijo MT, Vianna Novaes de Carvalho Teixeira A, et al.
824 Encapsulation in alginate-polymers improves stability and allows controlled
825 release of the UFV-AREG1 bacteriophage. *Food Res Int* 2021; **139**, 109947.
826 https://doi.org/10.1016/j.foodres.2020.109947.

827 Singla S, Harjai K, Chhibber S. Susceptibility of different phases of biofilm of
828 *Klebsiella pneumoniae* to three different antibiotics. *J Antibiot* 2013; **66**, 61–66.
829 https://doi.org/10.1038/ja.2012.101.

830 Stahlhut SG, Struve C, Krogfelt KA, et al. Biofilm formation of *Klebsiella*
831 *pneumoniae* on urethral catheters requires either type 1 or type 3 fimbriae. *FEMS*
832 *Immunol Med Microbiol* 2012; **65**, 350–359. https://doi.org/10.1111/j.1574-
833 695X.2012.00965.x.

834 Stepanovic S, Vukovic D, Dakic I, et al. A modified microtiter-plate test for
835 quantification of staphylococcal biofilm formation. *J Microbiol Methods* 2000; **40**,
836 175–179. https://doi.org/10.1016/S0167-7012(00)00122-6.

837 Sun X, Pu B, Qin J, et al. Effect of a Depolymerase Encoded by Phage168 on a
838 Carbapenem-Resistant *Klebsiella pneumoniae* and Its Biofilm. *Pathogens* 2023;
839 **12**, 1396. https://doi.org/10.3390/pathogens12121396.

840 Taha OA, Connerton PL, Connerton IF, et al. Bacteriophage ZCKP1: A Potential
841 Treatment for *Klebsiella pneumoniae* Isolated From Diabetic Foot Patients. *Front*
842 *Microbiol* 2018; **9**, 2127. https://doi.org/10.3389/fmicb.2018.02127.

843 Tang M, Wei X, Wan X, et al. The role and relationship with efflux pump of biofilm
844 formation in *Klebsiella pneumoniae*. *Microb Pathog* 2020; **147**, 104244.
845 https://doi.org/10.1016/j.micpath.2020.104244.

846 Tesfa T, Mitiku H, Edae M, et al. Prevalence and incidence of carbapenem-
847 resistant *Klebsiella pneumoniae* colonization: systematic review and meta-
848 analysis. *Syst Rev* 2022; **11**, 240. https://doi.org/10.1186/s13643-022-02110-3.

849 Vakili N, Asefnejad A. Titanium coating: introducing an antibacterial and bioactive
850 chitosan-alginate film on titanium by spin coating. *Biomed Tech* 2020; **65**, 621–
851 630. https://doi.org/10.1515/bmt-2018-0108.

852   Vieira Da Cruz A, Jiménez-Castellanos J, Börnsen C, et al. Pyridylpiperazine
853   efflux pump inhibitor boosts in vivo antibiotic efficacy against *Klebsiella*
854   *pneumoniae*. *EMBO Mol Med* 2024; **16**, 93–111. https://doi.org/10.1038/s44321-
855   023-00007-9.

856   Walker KA, Miner TA, Palacios M, et al. A *Klebsiella pneumoniae* Regulatory
857   Mutant Has Reduced Capsule Expression but Retains Hypermucoviscosity. *mBio*
858   2019; **10** https://doi.org/10.1128/mbio.00089-19.

859   Walker KA, Treat LP, Sepúlveda VE, et al. The Small Protein RmpD Drives
860   Hypermucoviscosity in *Klebsiella pneumoniae*. *mBio* 2020; **11**
861   https://doi.org/10.1128/mBio.01750-20.

862   Wu Y, Wang R, Xu M, et al. A Novel Polysaccharide Depolymerase Encoded by
863   the Phage SH-KP152226 Confers Specific Activity Against Multidrug-Resistant
864   *Klebsiella pneumoniae* via Biofilm Degradation. *Front Microbiol* 2019; **10**, 2768.
865   https://doi.org/10.3389/fmicb.2019.02768.

866   Xiao J, Zhu Y, Liu Y, et al. A composite coating of calcium alginate and gelatin
867   particles on Ti6Al4V implant for the delivery of water soluble drug. *J Biomed*
868   *Mater Res B Appl Biomater* 2009; **89B**, 543–550.
869   https://doi.org/10.1002/jbm.b.31246.

870   Yan Q, Zhou M, Zou M, et al. Hypervirulent *Klebsiella pneumoniae* induced
871   ventilator-associated pneumonia in mechanically ventilated patients in China. *Eur*
872   *J Clin Microbiol Infect Dis* 2016; **35**, 387–396. https://doi.org/10.1007/s10096-
873   015-2551-2.

874   Yang H, Chen Y, Cai Y, et al. A feasible strategy of Ag nanoparticles-sodium
875   alginate-polyacrylamide-polyvinyl alcohol hydrogel coatings for preventing
876   catheter-associated urinary tract infections. *Prog Org Coat* 2024; **196**, 108706.
877   https://doi.org/10.1016/j.porgcoat.2024.108706.

878   Yukgehnaish K, Rajandas H, Parimannan S, et al. PhageLeads: Rapid
879   Assessment of Phage Therapeutic Suitability Using an Ensemble Machine
880   Learning Approach. *Viruses* 2022; **14**, 342. https://doi.org/10.3390/v14020342.

881   Zhang M, Zhao X. Alginate hydrogel dressings for advanced wound
882   management. *Int J Biol Macromol* 2020; **162**, 1414–1428.
883   https://doi.org/10.1016/j.ijbiomac.2020.07.311.

884   Zhou Y, Xu D, Yu H, et al. Encapsulation of *Salmonella* phage SL01 in
885   alginate/carrageenan microcapsules as a delivery system and its application in
886   vitro. *Front Microbiol* 2022; **13**, 906103.
887   https://doi.org/10.3389/fmicb.2022.906103.

888   Zurabov F, Glazunov E, Kochetova T, et al. Bacteriophages with depolymerase
889   activity in the control of antibiotic resistant *Klebsiella pneumoniae* biofilms. *Sci*
890   *Rep* 2023; **13**, 15188. https://doi.org/10.1038/s41598-023-42505-3.

891

Author contributions statement

893   Conceptualisation: HRA & DN. Data curation: HRA, CVA & DN. Formal analysis:

894   HRA, CVA & DN. Funding acquisition: HRA, CVA & DN. Investigation: HRA, CVA &

895   DN. Methodology: HRA, CVA & DN. Supervision: DN. Writing – reviewing and

896   editing: HRA, CVA & DN.

897

898

899
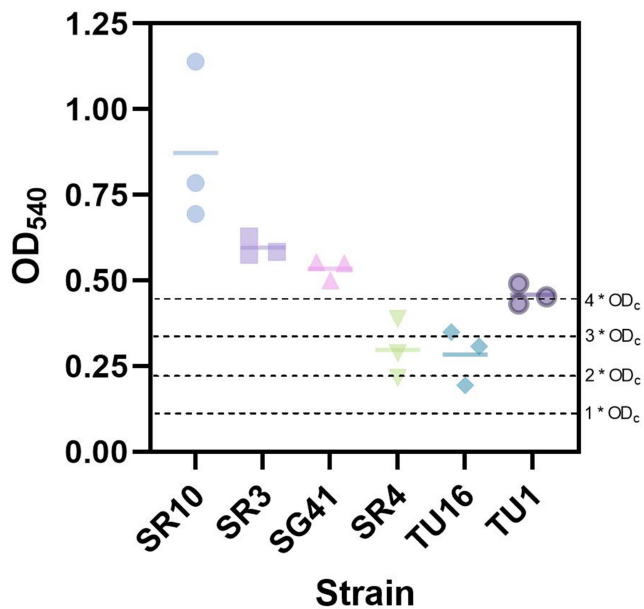
Figure 1. Biofilm-forming abilities of the strains used in this study. Biological (*n*=3)

and technical (*n*=4) replicates were performed for all strains. The mean of each

isolate's OD quadruplicate readings (OD_i) was calculated and compared with the

control cut-off OD (OD_C), which was defined as three standard deviations (SD)

above the mean of the negative control (3SD + mean). The amount of biofilm formed

was scored as non-adherent ($OD_i \leq OD_C$), weakly adherent ($OD_C < OD_i \leq 2\ OD_C$),

moderately adherent ($2\ OD_C < OD_i \leq 4\ OD_C$) or strongly adherent ($4\ OD_C < OD_i$).

907

908
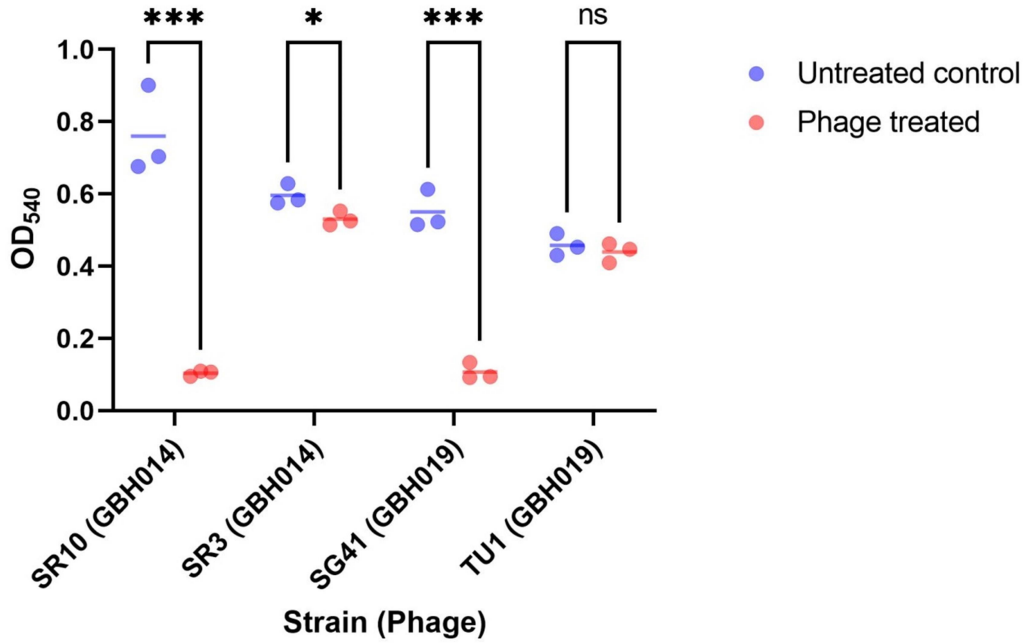
909

910 **Figure 2.** The ability of phages GBH014 and GBH019 to prevent biofilm formation by

911 *K. pneumoniae* strains identified as strong biofilm formers. Statistical significance of

912 the differences in biofilm formation of strains in the presence and absence of phage

913 was assessed using unpaired *t* test. Data are shown as mean for four technical and

914 three biological replicates per strain. * P = <0.05, ** P = <0.005, *** P = <0.0005.

915

916
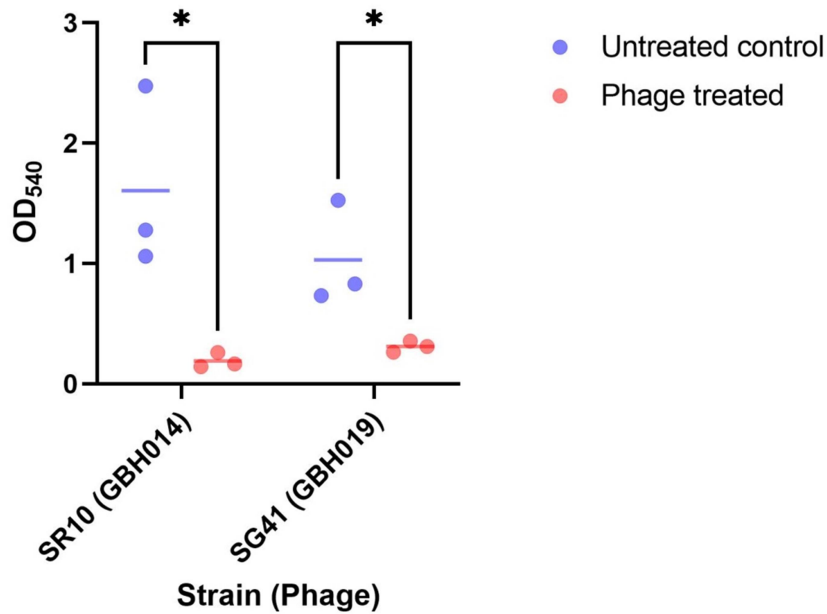
917

918   **Figure 3.** The ability of phages GBH014 and GBH019 to disrupt established biofilms

919   formed by *K. pneumoniae* strains SR10 and SG41. Statistical significance of the

920   differences in biofilm formation of strains in the presence and absence of phage was

921   assessed using unpaired *t* test. Data are shown as mean for four technical and three

922   biological replicates per strain. * P = <0.05.

923

924
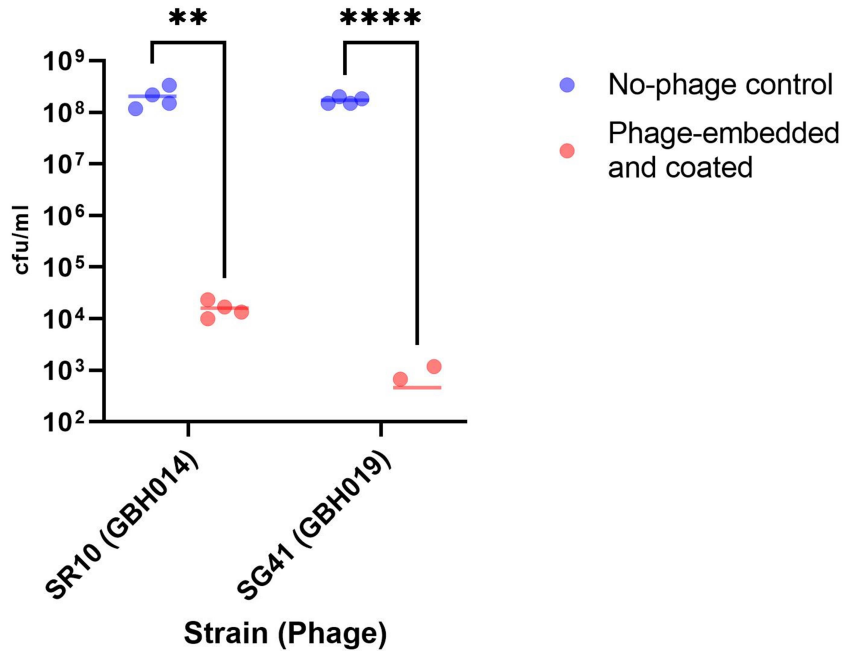
925

926 **Figure 4.** Antibiofilm properties of phage-embedded and coated alginate hydrogels.

927 Phage-embedded and coated alginate hydrogels were inoculated with *K.*

928 *pneumoniae* and the cfu ml^{-1} of any biofilm formed was determined following

929 incubation at 37°C for 24 h. Statistical significance of the differences in biofilm

930 formation between alginate hydrogels embedded and coated with phage versus

931 hydrogels without phage was assessed using unpaired *t* test. Data are shown as

932 mean for three technical and four biological replicates per strain. Only two biological

933 replicates are shown for Strain SG41 treated with GBH019 as the cfu ml^{-1} for two of

934 the biological replicates fell below our limit of detection of 100 cfu ml^{-1}. * P = <0.05, **

935 P = <0.005, *** P = <0.0005, **** P = <0.00005.

936

937
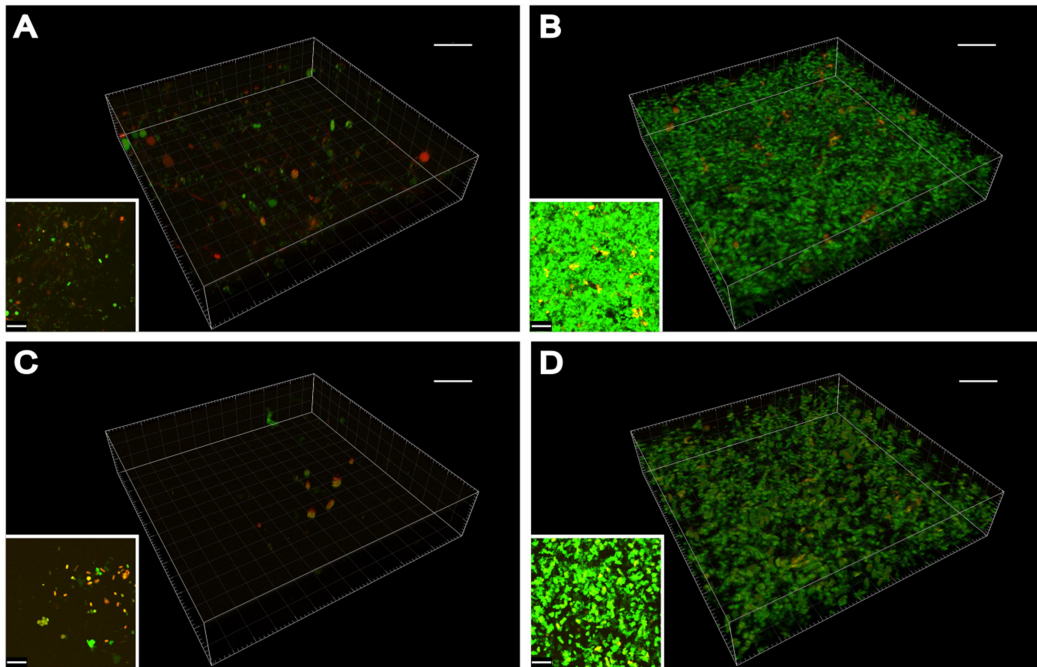
938

939 **Figure 5.** Antibiofilm properties of phage-embedded and coated alginate hydrogels

940 visualised by **c**onfocal laser scanning microscopy (CLSM). The images show

941 *Klebsiella* biofilms formed on alginate matrices stained with Syto9 (green, viable

942 cells) and propidium iodide (red, dead cells). Each panel presents the first 15 μm of

943 the biofilms, alongside a maximum intensity projection (bottom left) of a

944 representative Z-stack image. Images are a merge of the red and green channel.

945 Scale bars = 10 μm. **A.** *K. pneumoniae* SR10 biofilm formed on alginate embedded

946 and coated with phage GBH014. **B.** *K. pneumoniae* SR10 biofilm formed on alginate

947 in the absence of phage. **C.** *K. pneumoniae* SG41 biofilm formed on alginate

948 embedded and coated with phage GBH019. **D.** *K. pneumoniae* SG41 biofilm formed

949 on alginate in the absence of phage.

950

951
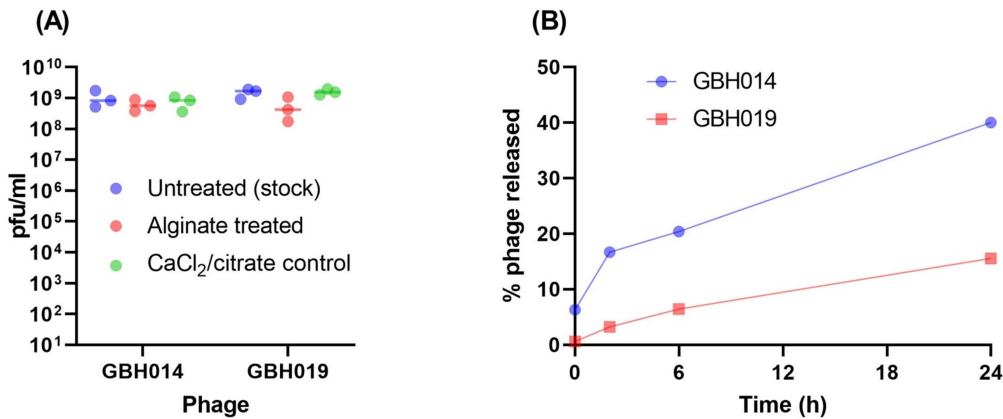
952

953 **Figure 6**: **(A)** Effect of alginate treatment on phage viability. Phage GBH014 or

954 GBH019 (original stocks at 1×10^9 pfu ml^{-1}) were incorporated into alginate hydrogels.

955 The gels were subsequently dissolved and the total number of viable phage

956 enumerated following alginate treatment. A control treatment of calcium chloride and

957 sodium citrate dihydrate (the reagents used to crosslink and disrupt the alginate gels,

958 respectively) was included. Data are shown as mean for three technical and three

959 biological replicates per phage. There was no statistically significant difference

960 detected between the treatment groups (Kruskal-Wallis, P = >0.05). **(B)** Release of

961 phage from alginate gels. Phage GBH014 or GBH019 were incorporated into

962 alginate hydrogels and the release of phage particles over a period of 24 h was

963 measured. Data are shown as the cumulative percentage of phage released from the

964 gel compared to the total number of phage recovered from dissolved gels at 0 h.

965 Data shows the percentage calculated from three technical and three biological

966 replicates per phage.

967

968

969

970   **Table 1**. *K. pneumoniae* strains used in this study. All strains were originally isolated

971   by Loraine *et al*., [16].

Strain	Species	Strain ID	Accession	KL	ST	Source
SR3	*K. pneumoniae*	4300STDY6470396	GCA_900493765.1	KL2	14	Pus
SR4	*K. pneumoniae*	4300STDY6470397	GCA_900493695.1	KL10	147	Sputum
SR10	*K. pneumoniae*	4300STDY6470403	GCA_900493775.1	KL2	65	Ascitic fluid
TU1	*K. pneumoniae*	4300STDY6542351	GCA_900493355.1	KL102	36	Pus
TU16	*K. pneumoniae*	4300STDY6542366	GCA_900493425.1	KL51	16	Urine
SG41	*K. pneumoniae*	4300STDY6636949	GCA_900492815.1	KL102	307	Blood

972

973

974

975 **Table 2**. Antibiotic susceptibility of *K. pneumoniae* isolates used in this study. Minimum inhibitory concentration, MIC; interpretation,

976 I; Resistant, R; susceptible, S; Ampicillin, AMP; Amoxicillin/Clavulanic acid, AMC; Piperacillin/Tazobactam, TZP; Cefazolin, CEZ;

977 Cefuroxime, CXM; Cefuroxime Axetil, CXMA; Ceftriaxone, CRO; Cefepime, FEP; Doripenem, DOR; Ertapemem, ETP; Imipemem,

978 IPM; Meropemem, MEM; Amikacin, AML; Gentamycin, GEN; Ciprofloxacin, CIP; Tetracycline, TET; Trimethoprim/Sulfamethoxazole,

979 SXT.

980

Strains	Antimicrobial																																			
	ESBL		AMP		AMC		TZP		CFZ		CXM		CXMA		CRO		FEP		DOR		ETP		IPM		MEM		AMK		GEN		CIP		TET		SXT	
	MIC	I	MIC	I	MIC	I	MIC	I	MIC	I	MIC	I	MIC	I	MIC	I	MIC	I	MIC	I	MIC	I	MIC	I	MIC	I	MIC	I	MIC	I	MIC	I	MIC	I	MIC	I
SR3	NEG	-	≥ 32	R	≥ 32	R	≥ 128	R	≥ 64	R	≥ 64	R	≥ 64	R	≥ 64	R	≥ 64	R	≥ 8	R	≥ 8	R	≥ 16	R	≥ 16	R	≥ 64	R	≤ 1	S	≥ 4	R	≥ 16	R	≥ 320	R
SR4	POS	+	≥ 32	R	≥ 32	R	≥ 128	R	≥ 64	R	≥ 64	R	≥ 64	R	≥ 64	R	≥ 64	R	≤ 0.12	S	≤ 0.5	S	≤ 0.25	S	≤ 0.25	S	32	I	≥ 16	R	≥ 4	R	≥ 16	R	≥ 320	R
SR10	NEG	-	≥ 32	R	≤ 2	S	≤ 4	S	≤ 4	S	2	S	2	S	≤ 1	S	≤ 1	S	≤ 0.12	S	≤ 0.5	S	≤ 0.25	S	≤ 0.25	S	≤ 2	S	≤ 1	S	≤ 0.25	S	≤ 1	S	≤ 20	S
TU1	NEG	-	≥ 32	R	≤ 2	S	≤ 4	S	≤ 4	S	4	S	4	S	≤ 1	S	≤ 1	S	≤ 0.12	S	≤ 0.5	S	0.5	S	≤ 0.25	S	≤ 2	S	≤ 1	S	≤ 0.25	S	≤ 1	S	≤ 20	S
TU16	NEG	-	≥ 32	R	4	S	≤ 4	S	≤ 4	S	4	S	4	S	≤ 1	S	≤ 1	S	≤ 0.12	S	≤ 0.5	S	≤ 0.25	S	≤ 0.25	S	≤ 2	S	≤ 1	S	≥ 4	R	≤ 1	S	≤ 20	S
SG41	POS	+	≥ 32	R	≥ 32	R	32	I	≥ 64	R	≥ 64	R	≥ 64	R	≥ 64	R	32	R	0.25	S	≤ 0.5	S	0.5	S	0.5	S	≤ 2	S	≤ 1	S	≥ 4	R	≥ 16	R	≥ 320	R

981

982

983

984

985

986

987